Dimensional Analysis and Laser-Ultrasonic Inspection of Cold Spray Additive Manufacturing Components

C. V. Cojocaru, P. Vo, D. Levesque, C. Bescond, M. Rivard, J. Boisvert, G. Lamouche, M. Martin, and E. Irissou

Abstract The use of cold spray (CS) in metal additive manufacturing (AM) offers well recognized advantages with typical commercial drivers being a rapid build rate, low process temperature and wide range of usable alloys. For cold spray, technology-specific considerations must be factored into each of the processing steps and in particular, an effective build strategy and toolpath are critical to moving towards near-net shape parts. Inspection and quality control of such complex parts is a challenge and new strategies have to be developed. For this purpose, this study looks to combine optical techniques for dimensional analysis with laser ultrasonics for volume probing.

Keywords Cold spray · Metal additive manufacturing · Non-destructive testing · Dimensional analysis · Laser ultrasonics

1 Introduction

The use of the cold spray in metal additive manufacturing (AM) offers several attractive competitive advantages in comparison with other additive techniques. Typical commercial drivers are rapid build rates, which can be on the order of kg/h, and low process temperatures that are well below material melting points [1]. Also, a wide range of alloys can be employed. Several reviews of specific benefits and considerations for AM by cold spray are available [2–8]. Fundamentally, cold spray additive manufacturing (CSAM) can be considered as a direct energy deposition (DED) process, as the material is deposited on a surface in a layer-by-layer approach to building a 3D structure. Due in part to its inherent spray characteristics, however, CSAM to date has often employed a methodology of rapid material deposition, with or without masking, into relatively simple shapes and wide tolerances that can lead

C. V. Cojocaru (✉) · P. Vo · D. Levesque · C. Bescond · M. Rivard · G. Lamouche · M. Martin · E. Irissou
National Research Council of Canada, 75 de Mortagne Blvd., Boucherville, QC J4B 6Y4, Canada
e-mail: cristian.cojocaru@cnrc-nrc.gc.ca

J. Boisvert
National Research Council of Canada Ottawa, 1200 Montreal Rd, Ottawa, ON K1A 0R6, Canada

S. Pathak and G. C. Saha (eds.), *Cold Spray in the Realm of Additive Manufacturing*, Materials Forming, Machining and Tribology,
https://doi.org/10.1007/978-3-030-42756-6_8

to constraints in part geometries and/or significant post-spray machining. Thus for cold spray, technology-specific considerations must be factored into each of the processing steps, and in particular, an effective build strategy and toolpath are critical to moving towards near-net-shape parts. These aspects are briefly addressed in Sect. 2 of this chapter. Inspection and quality control of such complex parts is a challenge, and new strategies have to be developed not only for off-line but also for on-line inspection. For this purpose, this study looks further to combine optical techniques for dimensional analysis with laser ultrasonics for volume probing of cold sprayed 3D structures. Dimensional measurements can be performed at various intermediate stages during the buildup of an intricate part, showing the value of in-process monitoring. In Sect. 3, various optical techniques for dimensional analysis are presented and compared: triangulation, structured-light and Optical Coherence Tomography (OCT). All techniques provide good results; nevertheless, OCT presents the advantage of requiring a single point-of-view compared to the two other techniques. This allows for the design of a compact scanner well suited for online process monitoring. Laser ultrasonics technique (LUT) is very attractive due to its non-contact nature and is well adapted to online implementation. In this context, we discuss in Sect. 4 non-destructive inspection performed off-line on metallic parts produced by the CSAM process. Laser ultrasonics is used to detect flaws using the synthetic aperture focusing technique (SAFT), and through-thickness distributed porosity is investigated using the backscattered signal. Also, laser shockwave is used to characterize bond strength at the interface between the cold spray deposits and the substrate. Inspection results from either the top layer or the underside of the substrate are presented. Laser-ultrasonic measurement can also be performed during post-heat treatment of cold spray AM metallic parts to capture microstructural and phase changes.

Work presented throughout the chapter stems from the activities carried out by the *National Research Council of Canada* within its *Cold Spray Additive Manufacturing Industrial R&D group* (*CSAM*). Among the efforts undertaken to develop 3D build-up capabilities and process windows to deposit new materials for cold spray, online and off-line testing of the deposits were identified as essential R&D avenues to deliver a robust AM process.

2 Development of Build Strategies and Advanced Toolpath Generation

In this section, we present a layer-by-layer build strategy and toolpath planning for producing more complex geometries and improving shape fidelity. The toolpath planning and programming required to build 3D structures with complex geometry and low (overspray) tolerances intrinsically need precise manipulation of the spray gun or part as applicable. This can often introduce an added layer of complexity versus that required for typical cold spray applications, which can often be programmed manually by a skilled operator using the robot teach pendant. Coating a surface, for

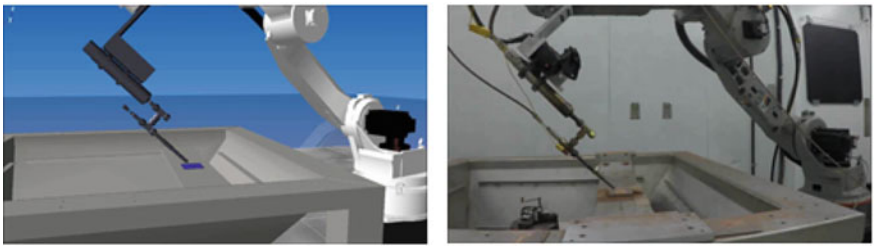

(a) (b)

Fig. 1 **a** Simulated and **b** spray setup

example, commonly employs a straightforward x-y index for stationary substrates or a linear displacement along the axis of rotating substrates.

Very similarly to other techniques such as laser-cladding, wire-arc additive manufacturing, etc., cold spray requires a digital thread to successfully build a 3D part starting from its 3D digital model. This thread includes the following steps: (i) generation of a part 3D model through CAD software and/or 3D scanning; (ii) slicing in a suitable orientation; (iii) path planning for each layer; and (iv) generation of machine codes. This needs different software to be achieved, and additional steps can be introduced, such as design optimization, manufacturing process simulation, etc. The use of software-based robot code programming provides flexibility and efficiency in toolpath planning as changes in path type, path sequencing, point density, etc. are more easily generated for evaluation. In addition, the simulation capabilities provided by commercial codes are often useful for verification and troubleshooting of build plans, e.g., collision avoidance, robot workspace, etc., as depicted in Fig. 1.

However, some specifics have to be considered in the development of build strategy and path planning in order to successfully manufacture 3D structures with cold spray additive manufacturing, e.g.: (i) the profile of the deposited materials that leads to significant overspray if not corrected; and (ii) cold spray is a high deposition rate, continuous process that cannot be stopped or started instantaneously. We will briefly explain these two points and see later how they can interfere with the overall manufacturing process.

2.1 Profile Control

With a basic cold spray setup, variations in the gas/particle flow across the diameter of a nozzle often manifest in a well-known tapering of the sides of a deposit. A ‘basic’ setup here refers to a standard commercial nozzle with axisymmetric geometry, no masking, and typically spray to a substrate surface. A typical deposit formed after repeated gun traverses along a single line of travel showed this tapering effect, Fig. 2a. Beyond a threshold number of traverses, deposition no longer occurred as

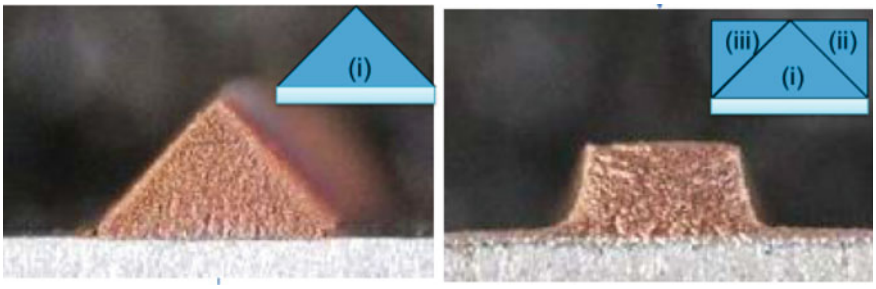

Fig. 2 Typical and altered deposit profiles: Cu sprayed at multiple angles to the substrate surface

the impact angles became increasingly off-normal, e.g., impacting the angled sides of the triangular deposit. In practice, this deposition profile effectively limits edge precision, and forces spray of a significantly larger footprint than required by designs as the tapering propagates with each additional layer, i.e., tapered edge grows as deposit thickness increases. This results in drawbacks such as significant amounts of excess material sprayed for large parts and a relatively large minimum size for fine, as-sprayed features. In order to limit these drawbacks, spray angles can be changed to avoid off-normal impacts, as in the case of producing vertical walls [2].

Profile alterations for line deposits of Cu were produced using a succession of spray angles, Fig. 2b. A rectangular profile was obtained for the Cu line deposit by spraying repeated passes normal to the substrate followed by repeated, alternating passes at ±45°. The starting deposit profile was dependent on materials, nozzle (equipment), process conditions, etc. However, spray angles and/or positions were adjusted accordingly to perform profile alterations.

The development of unique toolpaths for every type of material deposit can be resource-intensive, requiring extensive experimentation and/or modelling. One approach to simplify toolpath planning is to employ a standard set of toolpaths for profile alteration, e.g., successive spray angles normal and ±45° to the substrate. This method can be implemented in a straightforward manner and designs adjusted accordingly. While efficient in practice, there are potential tradeoffs in terms of build accuracy and deposit properties if starting profiles deviate significantly. Consequently, a more practical approach was taken, which balanced these two extremes; the development of different sets of toolpath combinations that produced specific, predictable profile alterations from typical starting deposit profiles.

In a general layer-by-layer approach, it is important to note that the toolpaths employed for an alteration of the layer profile maintain similar spray conditions to that used to build the body of the layer. With spray angles maintained normal to a target surface (e.g., spray at 45° to the substrate is equivalent to normal direction from the triangle edge in Fig. 2), deposit properties for both the layer fill and alteration should be similar. Full characterization is an area of further investigation to validate that the profile alterations do not degrade performance.

2.2 Spray Path Planning

A build within each layer is deconstructed into two sub-layer structures, which are labelled as layer filling and layer alteration in the schematic, Fig. 3. We explained above how critical the layer alteration step is in order to improve the dimensional accuracy of the build and limit the needs for further machining. The path planning for this is most often reduced to a single trajectory, or a set of trajectories, that follows the profile of all open contours, with an adapted angle versus the base substrate surface. The layer fill refers to depositing material for the body of part, which is analogous to producing cold spray AM parts by spraying oversized deposits. Similar to what is seen in pocket milling with CAM software, different paths can be considered to cover the very same surface, i.e. zig-zag toolpath; zig toolpath; contour parallel toolpath; spiral-type toolpath. The decision on the type of toolpath can be related to the shape of the surface to fill but is also influenced by the second point mentioned in the specifics of cold spray, i.e. the fact that cold spray is a high build rate, continuous process. Bearing in mind that, for a constant powder feed rate, the deposited thickness is directly related to the traverse speed of the cold spray equipment over the substrate surface (or the substrate traverse speed under the cold spray gun, depending on what the robot is manipulating), the toolpath has to be generated with a proper strategy to minimize robot acceleration/deceleration and sharp direction change. For this reason, spiral-type toolpaths are often preferred versus zig-zag-type. Small radius turns, and intersections also represent challenges as they can lead to significant layer thickness variations that interfere with the continuation of the build sequence.

It is important to emphasize that although specific layering strategies are dependent on the design, the reverse also applies. A good design can greatly facilitate a

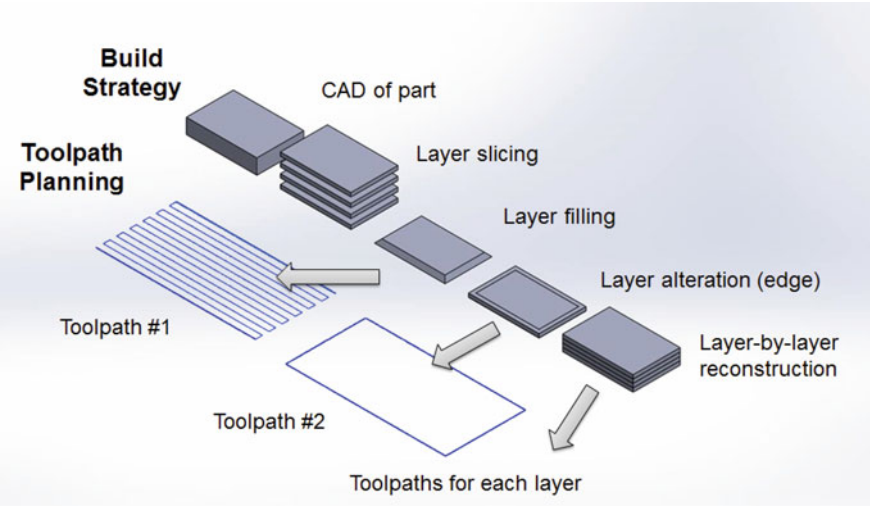

Fig. 3 Schematic of build strategy

cold spray build by simplifying the types of transitions and support structures that are required. The fabrication is also specific to materials, hardware, and process conditions and integration of these various elements is critical to a well-conceived, design-specific strategy.

Each sub-layer structure employs a different toolpath, with the complexity in toolpath planning heavily dependent on the geometries being produced. The toolpath accounts for the line-of-sight and proper access to the spray location. As build complexity increases and larger cold spray systems are used, this can become a significant challenge and designs become more constrained. In some cases, equipment changes, e.g., nozzles designed to produce uniform spray profiles, can be used to facilitate toolpath planning. The precision of a toolpath is also evaluated according to the design requirements as well as the capabilities of the manipulator (robot, gantry, etc.) and cold spray equipment (spray accuracy, process repeatability, etc.).

A layer-by-layer build strategy with profile alterations was employed to build several thin-walled features of copper on aluminum alloy substrates, Fig. 4. Figure 4a depicts the CAD drawings of such freeform stiffening structures and Fig. 4b the resulting cold sprayed structures.

The precision of the toolpath and process stability are two key factors in the uniformity of these as-sprayed features and comes in addition to layer thickness variations that could originate from variation in the traverse speed or from imperfect contour

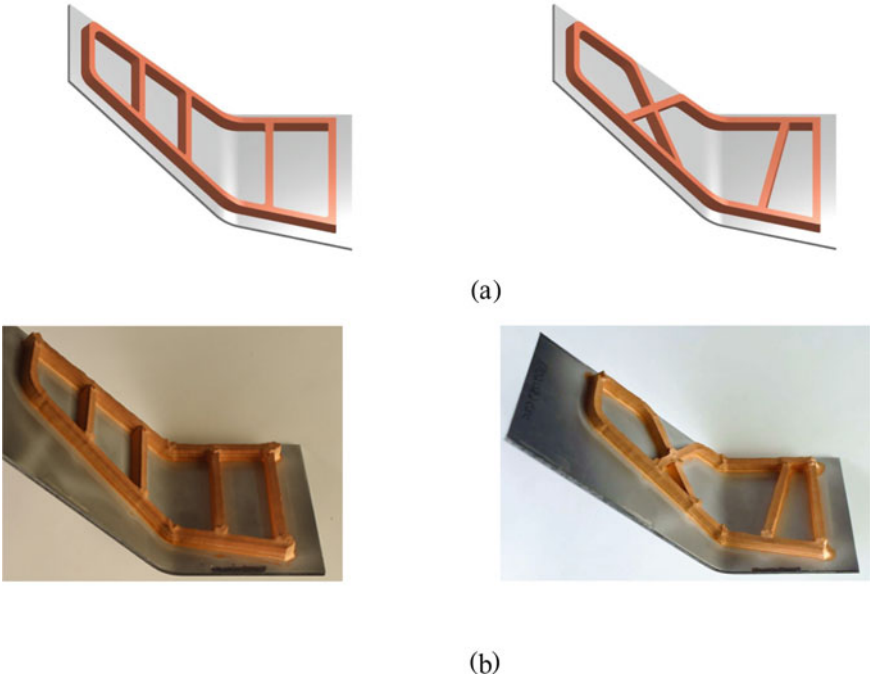

Fig. 4 **a** CAD drawings and **b** resulting in cold sprayed structures

correction. In the case of low build heights, those variations in the layer thickness might not be so detrimental that they could cause the failure of the build. However, when more complex builds are intended, with tens of layers, these variations can become critical.

While improving the general stability of the process and carefully planning the path for the entire build would resolve many of these issues, having a solution to monitor online the geometry of added features and furthermore their quality (through representative properties assessment) is paramount. Such solutions could be used to tailor the toolpath as a correction of past variations, and even repair during build defaults. The next sections will present some advancements in the development of such diagnostic tools.

3 Swept-Source Optical Coherence Tomography (SS-OCT)

In this section, we evaluate the capability of Swept-Source Optical Coherence Tomography (SS-OCT) technology to provide real-time monitoring of the dimensional characteristics of a part fabricated by the cold spray process. We first describe the SS-OCT technology and present results from quasi-online monitoring of the process described in the previous section, highlighting the value that could be added by online inspection. SS-OCT is then compared to other techniques that could allow dimensional monitoring and its advantages are highlighted. We end this section by demonstrating the ability of SS-OCT to characterize large parts produced by the cold spray process.

Optical Coherence Tomography (OCT) is an interferometric imaging technique which has been developed initially for biomedical imagery applications [9] but has great potential for the monitoring of industrial processes [10–12]. Modern implementations of OCT, Spectral-Domain OCT (SD-OCT) and Swept-Source OCT (SS-OCT) allow the performance of real-time tomography of non-opaque materials, enabling the dimensional characterization of internal structures as well as the detection of internal defects. These technologies can also be used to perform surface profilometry, providing the external dimensions of a part and the identification of surface defects. Industrial applications include monitoring of laser machining [13], laser welding [14], polymer-based [15] and metal-based [16] additive manufacturing.

Figure 5a presents a basic SS-OCT system in a Michelson configuration. The light emitted by a swept-laser is sent to a coupler using single-mode fibre. Light is split between a sample arm and a reference arm. For illustrative purposes, the sample arm contains three partial reflectors illuminated by a collimated beam. The collimated beam is a simplified representation; in a real SS-OCT system, the light is usually focused in the region of the sample. The reference arm contains a fixed mirror. The light beams reflected in both arms return to the coupler where they are recombined to interfere before being sent to a photodetector. The SS-OCT signal is composed of the interference pattern recorded by the detection system as the wavelength of the laser is swept. Figure 5b illustrates a typical interference pattern referred to as

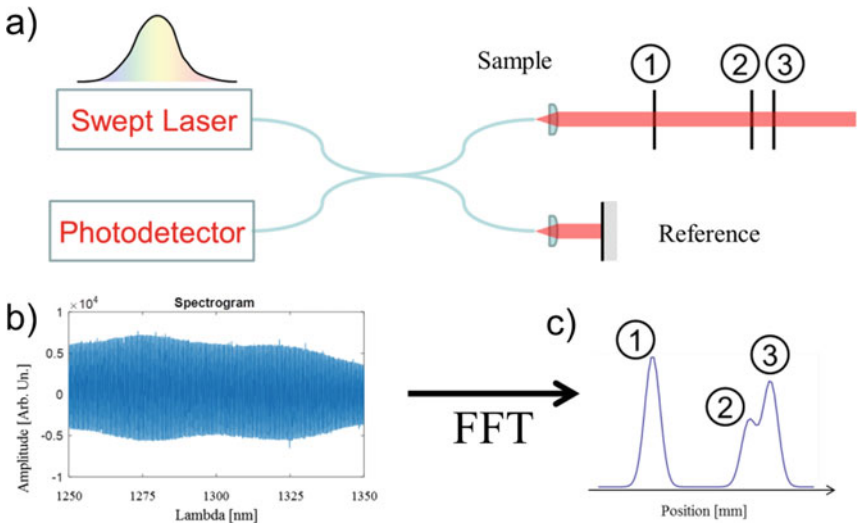

Fig. 5 **a** SS-OCT system. **b** Recorded interferogram signal. **c** Recovered sample structure after fast Fourier transform of the interferogram

a spectral interferogram. The location of any structure reflecting light in the sample arm is recovered from a fast Fourier transform (FFT) of the interferogram. This is illustrated in Fig. 5c where the three peaks provide the locations of the three partial reflectors in the sample arm.

When performing industrial monitoring, an optical scanning system is used in the sample arm to scan the surface of the part. A significant advantage of SS-OCT is that it requires a single point-of-view; a compact scanner can be designed to access any location, even hard-to-reach locations like corners and holes. Additionally, the scanner in the sample arm is connected to the other system components through an optical fibre and a few electrical wires. The scanner can thus be located close to a part while the other system components can be located away, at a more convenient location. This is a crucial feature when developing an online monitoring system for a challenging environment like the one found in the cold spray process.

Swept-lasers offered on the market today allow the design of SS-OCT systems that can achieve several hundreds of thousands of measurements per second. For 3D surface profilometry applications, that means several hundreds of thousands of points per second. This measurement rate is in the right order of magnitude for online monitoring of industrial processes.

3.1 *Quasi-online Measurements*

Quasi-online measurements were performed to demonstrate the added value of performing dimensional characterization while a part is built with the cold spray process. The experimental setup is illustrated in Fig. 6. Figure 6a shows the SS-OCT main unit, which was located just outside the spray booth. A one-dimensional galvanometer optical scanner was used to scan the surface of the part. The scanner was located within the spray booth and connected to the main OCT unit by an optical fibre and electrical wires passing through the wall of the spray booth. The part under fabrication was manipulated by a robot that moved the part between the fabrication location and the measurement location. At the fabrication location, the part was moved by the robot under the fixed nozzle, at a speed and orientation required by the spray pattern. At the measurement location indicated in Fig. 6b, the sample was translated by the robot in one direction while being scanned in a perpendicular direction by the optical scanner. These directions are indicated by the blue and red arrows in Fig. 6b. SS-OCT measurements were performed at a rate of 30,000 measurements per second. The optical scanner allowed 50 line profiles per second over a width of 15 mm, each line profile containing 600 points. The spacing between the line profiles was 0.05 mm, as dictated by the speed of the robot translation of 2.5 mm/s.

A rectangular ridge structure (freeform stiffening structure) was fabricated following the procedure described in the cold spray building strategy section with spray parameters that were far from optimal so as to provide challenging fabrication conditions, leading to a ridge with irregular corners. The fabrication conditions were intentionally challenging to provide clear features in the surface profilometry. An SS-OCT surface profile was performed after every five layers. In order to simulate results which would have been obtained from online monitoring during the fabrication, all surface profile measurements should have been performed with the same

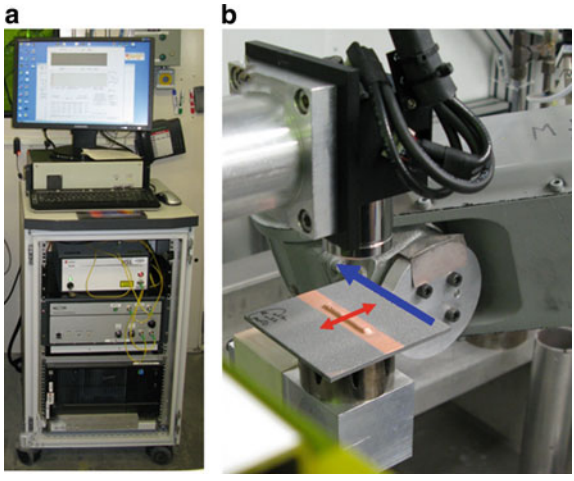

Fig. 6 Quasi-online setup. **a** OCT system. **b** OCT scanning head. The scan pattern is depicted by the red arrow. Robot movements are depicted by the blue arrow

angle as the one used for deposition. The measurement range of the SS-OCT system allowed measurements over a limited depth of 6 mm. This was not enough to capture the whole ridge structure for orientations of +45° and −45°, so surface profile measurements were performed at +20° and −20°. This is not a limitation of the technology, but a limitation of the specific SS-OCT system used for these measurements.

The surface profiles measured after each group of five layers are presented in Fig. 7. For each case, the bottom part shows the 2D rendering of the point cloud obtained with the PolyWorks software suite. The top left insert shows a line profile measured near the centre of the ridge while the top right insert shows a schematic representation of the structure after each five-layer step. Each surface profile is depicted with a specific colour and superimposed over the previous surface profiles. This gives a clear visualization of the contribution of each fabrication step towards the final structure and represents key information to optimize the fabrication process. When performed online, such information could allow process control through adjustments of the deposition parameters between each deposited layers. As an example, in the case shown in Fig. 7, it would have informed the operator to perform less than five layers for the two last steps which would have allowed a stop of the additive manufacturing process when the part reached a rectangle profile rather than overshooting to a trapezoid profile.

The added value of performing online monitoring to optimize the fabrication process is also illustrated in Figs. 7c, d. In Fig. 7c, the deposition at +45° created one sidewall of the ridge and overspray that results in a profile discontinuity to the

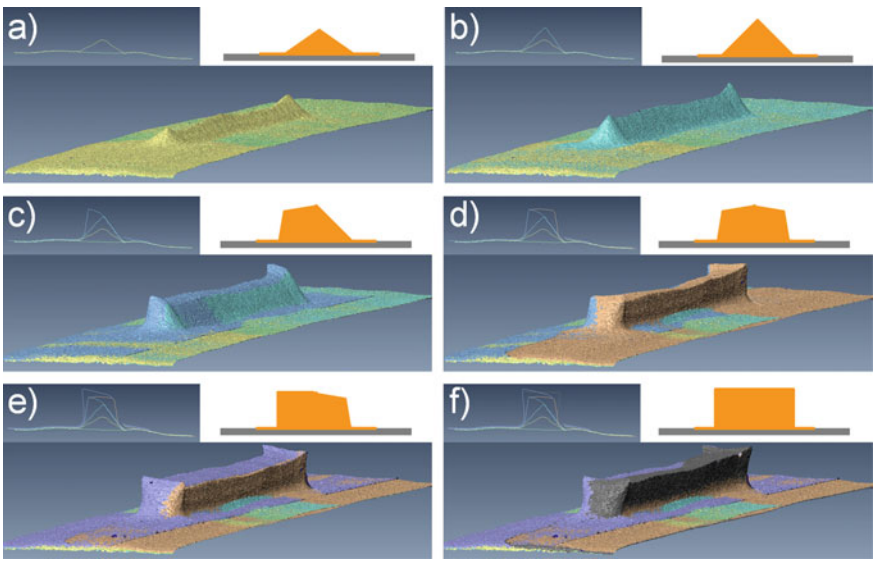

Fig. 7 Quasi-online measurement for fast deposition of a sample with a rectangular profile. **a**–**f** Point cloud surface, transverse profile and theoretical profile after successive fabrication steps

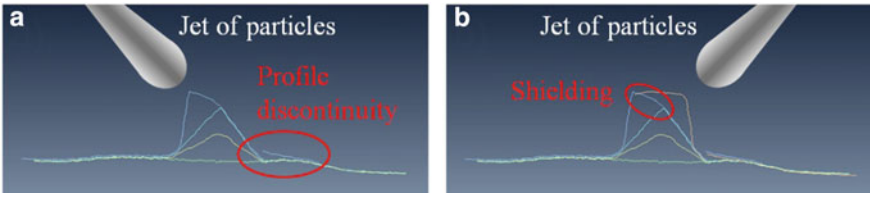

Fig. 8 **a** Sharp bump formed during fabrication, as seen in Fig. 7c. **b** The other side was shielded by the prior layer of material as seen in Fig. 7d

right of the ridge. As illustrated in Fig. 8a, this is caused by material being sprayed over the structure onto the base substrate. In Fig. 7d, the deposition at −45° created the other sidewall of the ridge. In that case, as shown in Fig. 8b, the previous layer insured shielding, so no material was sprayed over the structure to create a profile discontinuity on the left. Had online monitoring been performed between each layer, process parameters could have been adjusted as soon as the profile discontinuity creation of Fig. 7c was detected in order to minimize this unwanted feature.

3.2 Comparison with Other Techniques

Due to the nature of the fabrication process, only non-contact techniques should be considered to develop an online dimensional monitoring system with optical techniques being prime candidates. The surface roughness of parts produced by cold spray is large enough to ensure that any optical technique that relies on diffuse reflection should be capable of performing a surface profilometry. Dimensions should be measured with an accuracy of the order of few microns. This is not a stringent requirement since such accuracy can be achieved with most of the optical techniques. The main criteria to select one technology over another is the ease of integration of the online monitoring system. The technology must also allow measurements over a range large enough to ensure that the whole structure is monitored, especially when measured from an angle.

To illustrate a variety of optical techniques that could be employed, we performed measurements on the same part using SS-OCT, triangulation and structured light. The test sample contained 6 stripes representing various steps in the fabrication of a ridge structure. The dimensions of the sample were 56 mm × 77 mm and the largest stripe was 3.6 mm in width and 2.5 mm in height.

SS-OCT measurements were performed at a rate of 142,000 measurements per second with an illumination spot size of 100 μm (wavelength around 1.55 μm) over a scan width of 100 mm. The spot size provided a depth of field large enough which, combined with the large scan width, allowed the measurement of the whole sample at once. Scanning was performed with a galvanometer in one direction while the

sample was translated by a motorized stage in the other direction. Spacing between measurements points was about 25 μm in both directions.

Triangulation measurements were made with a laser scan triangulation (LST) system. The measurement rate was 60 kHz. The surface was scanned by a galvanometer over a surface of approximately 30 mm × 20 mm, with spacing between measurement points of 10 μm in both transverse directions. The restricted measurement area is not a limitation of the technology, but a feature of the specific system used. The illumination spot size was 20 μm (wavelength of 405 nm). The system was equipped with an adaptive focusing system.

Structured light imaging does not require a surface scan; instead, it measures all the points in the field of view in parallel. Measurements were performed with a system capable of providing 24 million 3D points per second. Sections of approximately 21 mm × 28 mm were measured with a spacing of 7 μm in both directions between measurement points. The system used a LED source centered at 525 nm and was calibrated over 3 mm around the focal point.

We do not provide here the detailed analysis of the results as all techniques did perform well for these offline measurements. Figure 9a shows the SS-OCT surface profile measured in one shot over the whole surface sample from a normal (0° incidence) point of view. All points of the surface are clearly visible, except for the sharp edges of the large ridge structures on the right; the light was coming from above, travelling parallel to the edges, making ridge wall surface measurement very challenging. In Fig. 9b, structured-light measurements are overlaid over the SS-OCT point cloud. The whole structure was not imaged with the structured light system at once. Three measurements are shown in different colours. A cross section of the surface profiles

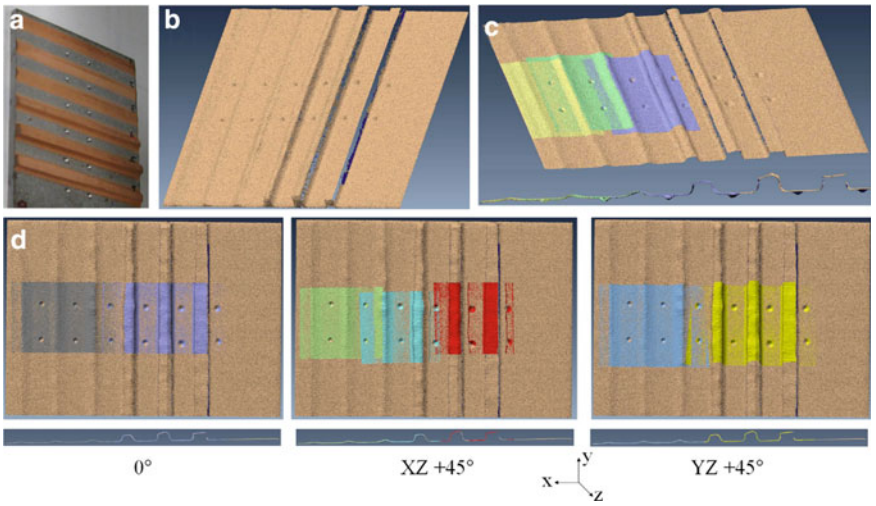

Fig. 9 CSAM copper ridges sample scanned with three different profilometry imaging techniques. **a** Picture of round-robin CSAM copper ridges sample. **b** SS-OCT 0°. **c** Structured Light compared to SS-OCT. **d** Laser scan triangulation compared to SS-OCT

Table 1 Comparison of online imaging techniques attributes

	Laser line triangulation	Laser scan triangulation	OCT profilometry	Structured light (phase shift)
Measurement quality	+++	+++	+++	+++
Cost	$	$$	$$$	$$
Adapted to online measurement	+++	+++	+++	*
Speed	+++	+	++	++++
Parasite reflection handling		+	++	
Compactness	+	+	+++	*

is also shown below the point clouds. There is good agreement between both imaging modalities. Figure 9c compares the laser scan triangulation measurements with SS-OCT. Again, measurements performed over different areas are shown with different colours. Triangulation measurements are provided for a scanning performed from the normal of the surface (Z-axis), as well as for orientations tilted by $+45°$ in the XZ plane and tilted by $+45°$ in the YZ plane. Cross-sectional views of the profiles are provided under the point clouds. Again, there is good agreement between results obtained with SS-OCT and triangulation. One side of the ridge structures are not visible for triangulation measurements performed with orientations of $+45°$, a result which is expected and common to all-optical inspection techniques since the structures create shadowing when inspected from an angle.

Results of Fig. 9 confirm that the various optical measurement techniques can provide good results when performing an offline inspection of cold sprayed parts. The challenge resides in how efficiently these can be integrated into an online environment. This is addressed in Table 1, where the strengths and weaknesses of online monitoring are summarized for each technique. We have added Line Laser Triangulation (LLT) to the techniques considered above.

In terms of cost, SS-OCT is the most expensive technology, while LLT is the least. The cost of LST can vary, depending upon the complexity of the system since features like adaptive focusing can be used for enhanced capability, but these come at a cost. In terms of measurement speed, structured light is the most efficient since it provides the full 2d profile at once. LLT can easily reach a rate of 1000 line profiles per second. LST and SS-OCT both rely on scanning which can be a limitation, although they can both provide measurements rate large enough for cold spray online monitoring. All techniques have been implemented in various online monitoring applications, so nothing intrinsic to these technologies could prevent them from being used online. In the case of cold spray monitoring, the compactness of the sensor is an important aspect. Structured-light requires that the whole sample be visible at once and can only be used to inspect a layer after it is entirely deposited. LST and LLT both require two

points of views which requires space. One significant advantage of SS-OCT is that it requires a single point of view; the same optical path is used for both illumination and detection. This allows the design of very compact scanning heads which can be easily integrated with a fabrication system. The ability to handle parasite reflection is also important when fabricating complex parts. Multiple reflections can provide unwanted artefacts. LLT and structured light are more sensitive to these parasitic reflections. LST systems can be customized to handle parasitic reflections at the cost of a more complex system. SS-OCT provides a full measurement through depth. Parasitic reflections will lead to additional peaks in this depth profile. These peaks can easily be identified and disregarded, making SS-OCT robust regarding parasitic reflections.

3.3 Capacity to Measure Large Objects

OCT imaging was initially developed to take high-resolution images of small areas in biological samples. But, like other laser profilometry techniques, it can be suited to scan larger parts such as those shown in Fig. 10. These reinforcement-like structures measure 150 mm × 70 mm × 40 mm. The second sample was produced using the same cold spray process as the as-sprayed sample but underwent a machining fabrication step after cold spray deposition to smooth its surfaces. By stitching together two separate scans of a sample, the topography of the whole part can be reconstructed.

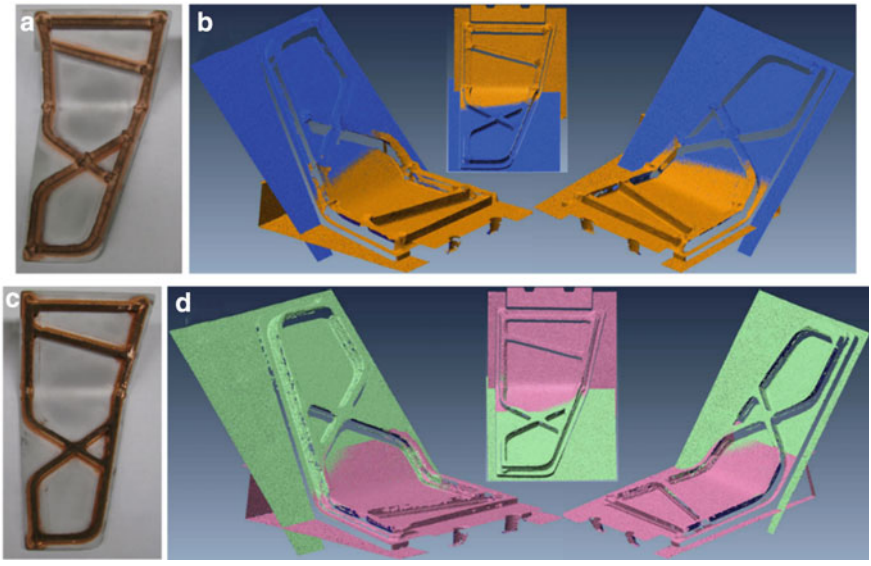

Fig. 10 OCT measurements of CSAM reinforcement-like structures. **a** Picture of the as-sprayed sample. **b** Stitched OCTscan. **c** Picture of the machined sample. **d** Stitched OCT scan

Additional scans from other points of view would be needed to capture the vertical surfaces on the part as well. Even larger parts could also be measured online using optical imaging techniques by tracking the position of the sensor relative to the part and through image stitching.

4 Laser-Ultrasonic Inspection of Cold Spray Additive Manufacturing Components

In this section, we present results of laser ultrasonic testing (LUT) performed off-line, on metallic structures deposited by the cold spray AM process. LUT was employed to detect flaws using the synthetic aperture focusing technique (SAFT) [17], and through-thickness distributed porosity was investigated using the backscattered signal [18]. The latter approach was applied in recent years to study porosity in composite materials [19], as well as grain shape and size distribution in steel [20–22]. Also, a laser shockwave technique was applied to characterize bond strength [23, 24] at the interface between the cold spray deposition and the substrate. Finally, for the post-heat treatment of cold spray AM metallic parts, we show an example of how LUT can be performed to capture the microstructural and phase changes. Inspection results from either the top layer or the underside of the substrate are discussed in the following.

4.1 Laser-Ultrasonic Inspection for Flaw Detection

Laser ultrasonics combined with SAFT was employed for the flaw, and porosity detection in Al cold spray coated samples. A set of three aluminum (Al) cold spray coatings deposited with conditions to intentionally produce different porosity levels was prepared. Figure 11a shows one such sample. Sample #1 (8.8 mm thick coating) has low porosity, sample #2 (5.5 mm thick coating) has an intermediate porosity and sample #3 (4.1 mm thick coating) has a high porosity with possible flaws present. Each coating is deposited on an Al6061 4.8 mm thick substrate.

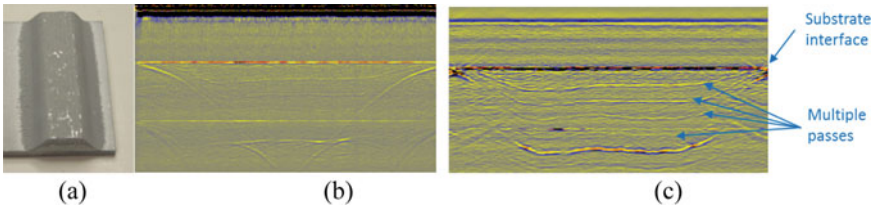

Fig. 11 **a** Photo of one Al/Al6061 cold spray sample used for testing. B-scans on Al/Al6061 sample #2 from the substrate, **b** raw data and **c** after SAFT reconstruction

For use with SAFT, the generation and detection zones overlapped at the surface for 1D or 2D scanning from either the top deposited layer or the underside of the substrate. Ultrasound generation was performed in the slight ablation regime (less than 1 μm) with a short pulse Nd:YAG laser in its 2nd harmonic (532 nm wavelength) to achieve high frequencies. For detection, a long pulse Nd:YAG laser (1064 nm wavelength) and a small spot size were used. The phase demodulator was a 1-m long confocal Fabry-Perot interferometer in reflection mode. Frequency content up to 80 MHz was successfully generated and detected in the above test samples. Mechanical scanning along single lines up to 30 mm length was performed for data acquisition of the waveforms with a step size of 0.1 mm. SAFT reconstruction was performed with an aperture angle of 30° and a frequency bandwidth from 1.5 to 80 MHz using the longitudinal mode.

Using the above test conditions, line scans were performed on the underside of the substrate of the three samples over a length of 30 mm (Fig. 11). B-scan images from the raw data and after SAFT reconstruction of a single scan line are shown respectively in Fig. 11b, c for sample #2 of intermediate porosity, starting with the substrate on top. Weak indications are observed from the raw data image, some of them as hyperbola shapes, and are more clearly resolved after SAFT reconstruction. The more or less continuous indications observed in Fig. 11c are attributed to imperfect contact between layers associated with the multiple passes of the cold spray AM at suboptimal spray conditions. Also, a strong indication of the substrate interface with the coating is apparent in both B-scan images. A similar indication of lower amplitude from the substrate is observed close to the last cold spray pass (bottom of B-scan), related to an echo propagating back and forth in the substrate. The longitudinal velocity difference between the Al alloy substrate and the Al coating is small and such reflections are more related to the bond integrity of the coating with the substrate. This is also investigated further later.

Figure 12a shows a B-scan image after SAFT reconstruction of a particular scan line from the coating side over a length of 15 mm. As expected, the continuous indications attributed to the multiple passes are observed while a bit less resolved.

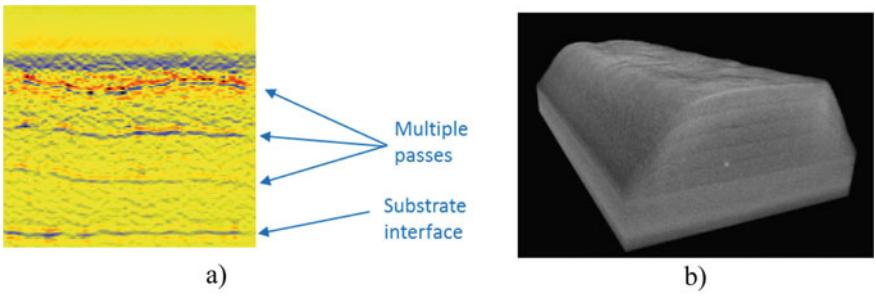

Fig. 12 **a** B-scan from coating after SAFT reconstruction for Al/Al6061 sample #2 and **b** corresponding X-ray μCT image

The indication between last cold spray passes on top of the coating is missing due to the blind zone related to the large surface displacement in laser-ultrasonic signals. A further investigation was made on these samples using X-ray μCT as well as a series of micrographs. Figure 12b shows an X-ray μCT image after processing the radiographic data. The agreement between the observations in this image and the laser-ultrasonic results is fairly good. Not shown here, the micrograph image shows porosity everywhere throughout the thickness, with a slightly larger pore concentration for the interface between each pass. This point is investigated in the next section.

4.2 Laser-Ultrasonic Backscattering for Porosity Evaluation

To further study porosity, the spectral analysis of the laser-ultrasonic backscattered signals obtained from the top surface of the coating was considered. Figure 13 presents the principle of measurement with the backscattered amplitude (BSA) spectrum after averaging 100 spectra from a line scan, and the decay slope in the spectrum estimated between the two cursors. As shown in Fig. 13, the BSA method can be applied over the full-time window between the large surface displacement and the first interface echo arrival, as an indication of average porosity found through the sample thickness. In a further study, an analytical model for backscattering [19, 20] could be developed to relate such decay slope with the porosity level.

Additionally, a sliding small time window of typically 0.6 μs can be applied in the same time interval to estimate the decay slope in successive BSA spectra. Using the single scattering hypothesis, the time window location can be associated with an

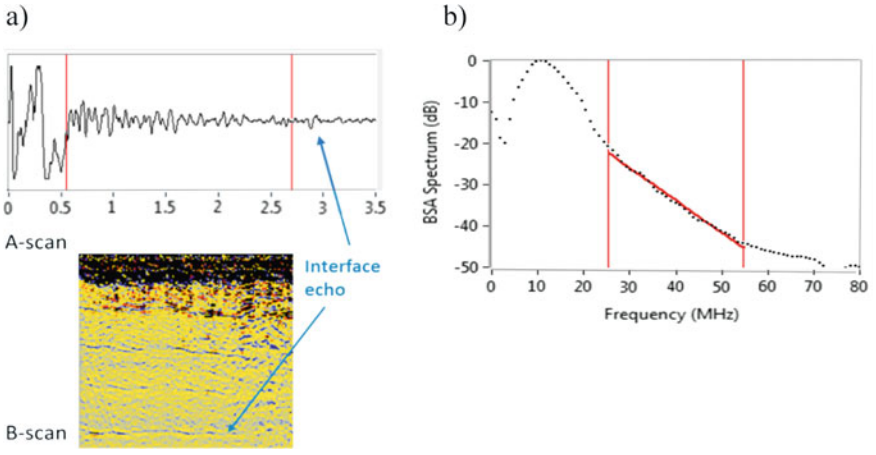

Fig. 13 Principle of the BSA method used. Example of **a** backscattered signal and **b** BSA spectrum after averaging and decay slope estimated between the cursors

equivalent depth, where the BSA decay slope indicative of local porosity is estimated. Figure 14 shows the BSA decay slope as a function of depth and Fig. 15 shows the series of micrographs analyzed through the thickness of the three Al/Al6061 cold spray samples. Compared to micrographs, consistent results are found between samples as well as through the thickness of each sample, with a larger negative slope corresponding to higher porosity near the top surface and a decreasing slope toward

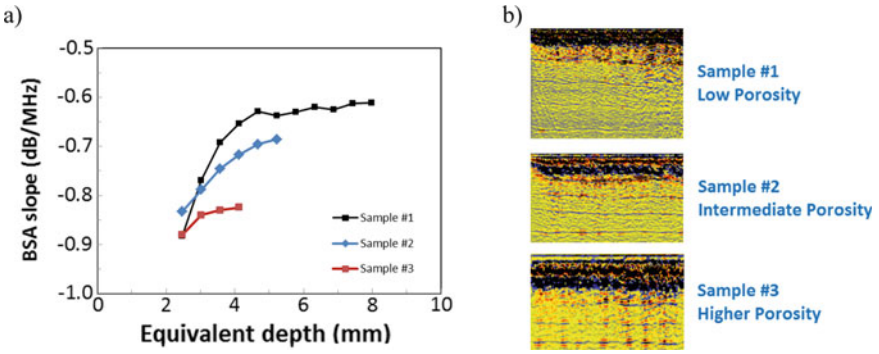

Fig. 14 **a** BSA decay slope as a function of depth through the thickness of the Al/Al6061 samples, and **b** corresponding B-scan images

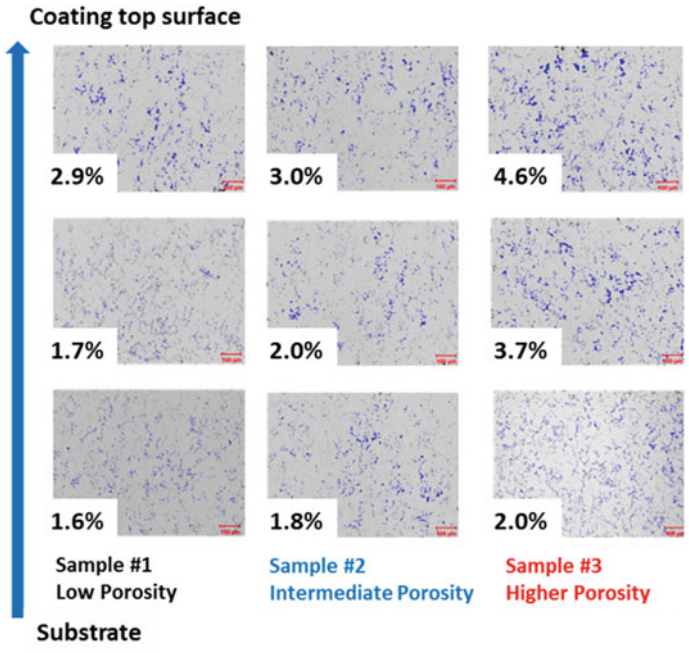

Fig. 15 Series of micrographs through the thickness of the Al/Al6061 samples

the substrate interface. Not shown here, an opposite behaviour (smaller to larger negative slope) is found scanning from the substrate side and analyzing backscattered signals after the interface echo.

While testing on a limited set of samples, the approach appears promising and will be further investigated. The method should work better when porosity near the surface is not too large to avoid a substantial reduction of the BSA signal deeper in the material. Also, the effect of multiple scattering should make the method not work well at typically more than 4–5 mm deep.

4.3 Laser-Ultrasonic/Shockwave for Bond Integrity Assessment

Another aspect to be considered with the cold spray AM process is the bond integrity between the coating and the substrate. This is particularly important for AM applications such as part reinforcement, dimensional restoration and structural repair. For these tests, a set of Al/Al6061 cold spray samples were prepared with a pulsed laser surface pre-treatment to improve the adhesion between the coating and the substrate [25].

Line scans were performed on the underside of the substrate of the cold spray samples over a length of 42 mm. B-scan images after SAFT reconstruction of a single scan line of 4 samples are shown in Fig. 16, starting with the substrate on top. A clear indication of the substrate interface with the coating is apparent in all cases but of variable amplitude. As in Fig. 11c, such reflections should be related to bond integrity and may vary depending on the surface treatment during the AM process. Also, there is a need to quantitatively determine the bond strength at the interface in each case.

For this purpose, a laser shockwave proof test method is considered with the principle shown in Fig. 17. With this technique, a high-energy pulsed laser produces a compressive large-amplitude wave at the top surface of the sample. The compressive shock wave travels through the sample and after reaching the lower surface, the compressive wave is changed by the free surface into a tensile wave that travels back through the sample. A shock wave amplitude that reaches over a certain threshold will create tensile stresses large enough to debond interfaces in the component. By

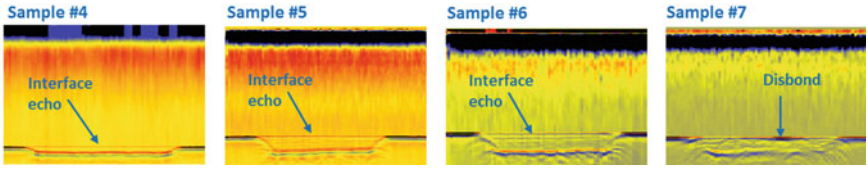

Fig. 16 B-scans from the substrate on the Al/Al6061 samples with surface treatment after SAFT reconstruction

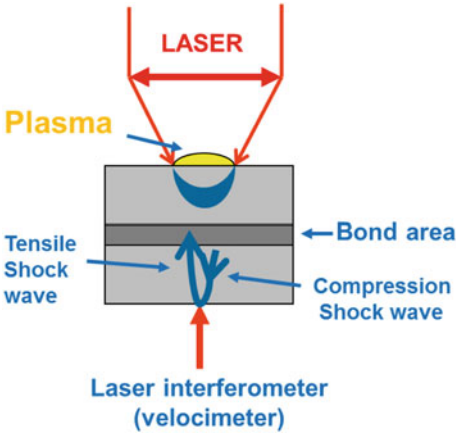

Fig. 17 Principle of the laser shockwave proof test

measuring the back surface velocity response with a Fabry-Perot etalon (velocimeter) [26] for different laser energy and using a model for shock wave propagation [27], the stress required to delaminate the coating from the substrate can be assessed. Figure 18 shows an example of such a calculation for one of the cold spray samples. Calculated stress values are generally larger than in quasi-static mechanical tests since laser shock wave measurement involves high strain rate, typically of 10^5–10^6 s^{-1}. To confirm that the system debonded the interface a post-shock laser-ultrasonic inspection is used to perform C-scan imaging of the sample. The debonded interface will keep the ultrasound from propagating to the backside of the sample, and this will be captured in the resulting image.

To determine bond strength a laser shockwave technique was applied on the cold spray AM samples #4–6 that do not present a disbond in Fig. 16. Laser energies from 0.2 to 2.2 J were tested at different locations from the substrate side of each sample. Figure 19 shows the back surface velocity from the velocimeter (on the coating) at

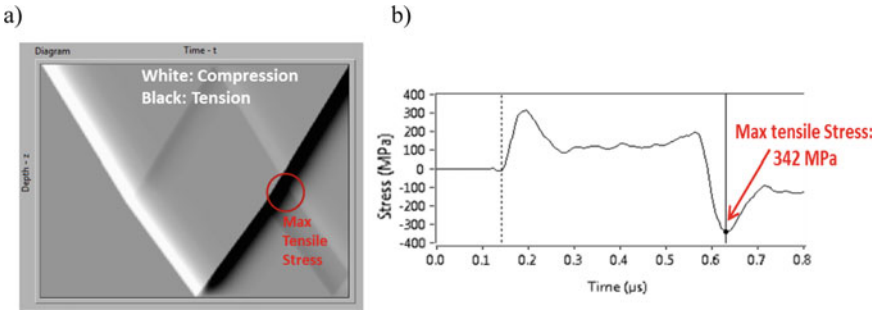

Fig. 18 Example of **a** ray tracing shock calculation with time-depth representation and **b** stress evaluated at the interface from measured back surface velocity

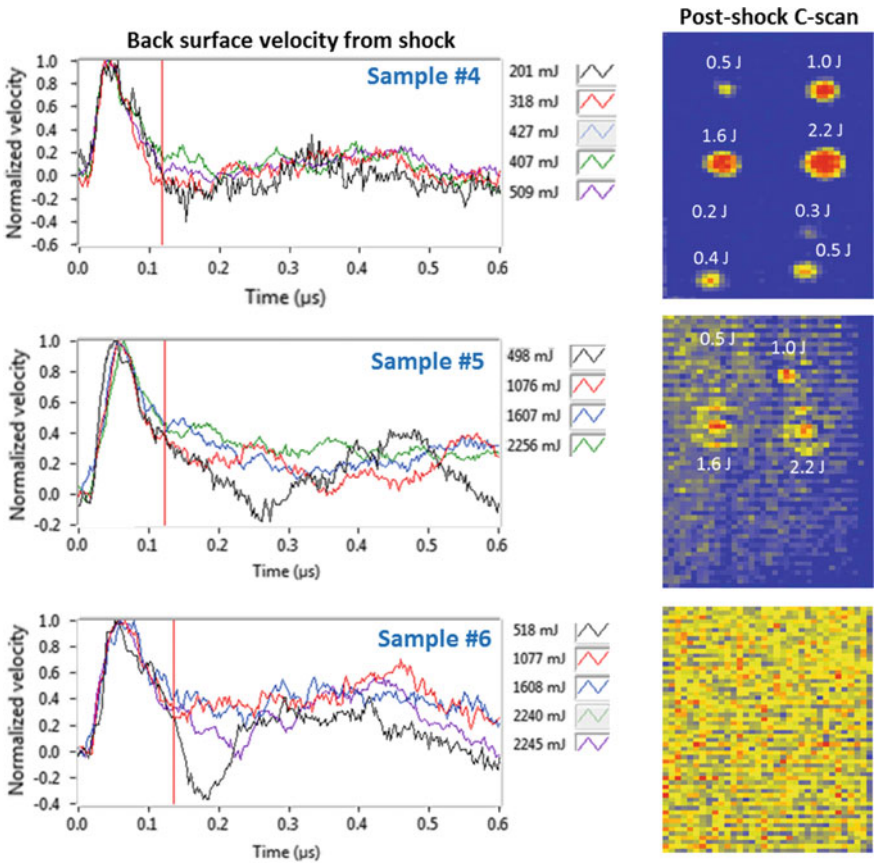

Fig. 19 Back surface velocity at different laser energies and post-shock laser-ultrasonic C-scans of the Al/Al samples

the different laser energies (indicated on the right of each graph) and the post-shock laser-ultrasonic C-scans on these samples. For sample #6, the bond did not open for the laser energies tested. The back surface velocity response at the threshold laser energy producing a disbond is then used to calculate stress at the interface. Stress values calculated for corresponding laser debonding energy are given in Table 2. A

Table 2 Calculated stress near debonding at the interface of the Al/Al alloy samples

Al/Al sample ID	Coating thickness (mm)	Debonding energy (J)	Min stress (MPa)	Max stress (MPa)
4	0.7	0.3	104	242
5	0.9	0.5	271	393
6	1.2	2.2+	358	N/A

more precise bond strength value could be obtained by testing each sample with more energy levels, but it may also vary from one location to another in the component.

4.4 Laser-Ultrasonic Monitoring During Heat Treatment

In some applications of cold spray AM, a post-heat treatment of the component is required. Laser-ultrasonic monitoring can be performed at high temperature during such heat treatment to understand better and optimize the occurrence of recrystallization, phase transformation, sintering, etc. As a first study, cold spray samples made of H13 tool steel on mild steel substrate were prepared. Then, the 3.3 mm thick H13 coating of each sample was detached from the substrate and inserted in a Gleeble machine for direct resistance heating. A laser-ultrasonic system, coupled with the Gleeble, was used to monitor the longitudinal velocity as a function of time and temperature. Such a system was developed in the past to study grain size evolution and phase transformation in steel [21, 22, 28–30].

Two different heat treatments are considered for these tests. Figure 20 shows the temperature history for the first heat treatment of long duration and corresponding ultrasonic velocity as a function of temperature on a stand-alone H13 sample. The ultrasonic velocity for the cold spray sample starts with a quite low value of 4.5 mm/μs and reaches 6.0 mm/μs after cooling, as expected for bulk H13 tool steel. Moreover, the ultrasonic velocity exhibits two changes in its behaviour near 550 °C and later at 800 °C. These changes are found attributable to the apparent effect of microstructural changes. The 550 °C is near a standard tempering temperature for H13 [31] while the 800 °C is near a phase change according to the H13 phase diagram [32]. Not shown here, the ultrasonic velocity during heating of short duration may show a quite different dynamic behaviour, and this has to be further investigated.

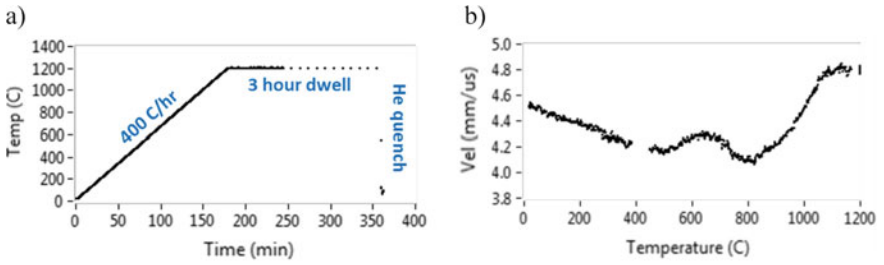

Fig. 20 **a** Temperature history of first heat treatment and **b** ultrasonic velocity as a function of temperature

5 Conclusions

To approach near-net shape features of cold spray some specific considerations with respect to deposit profile control and spray path planning must be considered. This was demonstrated by building freeform stiffening structures using a digital thread similar to other AM processes. The precision of the toolpath and process stability are two key elements in the uniformity of these as-sprayed features. While improving these factors for the entire build would resolve many issues, having a solution to monitor online, the geometry of added features and furthermore their quality, through representative properties assessment, is critical. The build requires both online and offline inspection.

A comparison of various dimensional inspection techniques, which all showed good results, prompted OCT as being the technique of choice for online inspection due to the compact scanning head design which can ultimately be easily integrated with a fabrication system. Moreover, since OCT provides full through-depth measurement, it is more robust regarding parasitic reflections than the other techniques presented. A quasi-online OCT measurement demonstrated the feasibility of implementation of the technique for real-time inspection, which allows adjustment of the spray parameters during the build.

It is equally essential to be able to perform remote inspection and to confirm the integrity of the sprayed part, e.g., porosity, adhesion, etc. Consequently, laser-ultrasonic testing was employed in a parallel investigation of a variety of cold sprayed samples. LUT, combined with SAFT, was used to detect flaws in Al/Al alloy samples from both the substrate and deposit sides (surfaces). Indications of multi-passes and variations in bond integrity with the substrate were observed. This was further validated by X-ray μCT showing larger pore concentration between each pass. Another aspect considered was capturing information regarding through-thickness distributed porosity using a spectral analysis of the laser-ultrasonic backscattered signal. Using a sliding time window a BSA decay slope was found promising to provide an indication of porosity variations through the sample thickness as confirmed by a series of micrographs. Also, the laser shockwave technique was used to characterize bond strength at the interface between the cold spray deposition and the substrate. Finally, laser-ultrasonic testing was shown to be useful to monitor microstructural changes such as phase changes, recrystallization and sintering phenomena during post-heat treatment of cold spray AM.

Acknowledgements This work has been conducted within the NRC's Cold Spray Additive Manufacturing Industrial R&D Group CSAM. The authors are grateful to Mr. M. Zeman and Mr. D. de Lagrave for their contribution in the sample preparation and performing the series of micrographs, as well as to Mr. C. Brosseau and Mr. M. Lord for their participation in the laser-ultrasonic measurements of the cold spray samples tested in this work.

References

1. Schmidt, T., Assadi, H., Gartner, F., Richter, H., Stoltenhoff, T., Kreye, H., & Klassen, T. (2009). From particle acceleration to impact and bonding in cold spraying. *Journal of Thermal Spray Technology, 18,* 794–808.
2. Pattison, J., Celotto, S., Morgan, R., Bray, M., & O'Neill, W. (2007). Cold gas dynamic manufacturing: A non-thermal approach to freeform fabrication. *International Journal of Machine Tools and Manufacture, 47,* 627–634.
3. Sova, A., Grigoriev, S., Okunkova, A., & Smurov, I. (2013). Potential of cold gas dynamic spray as additive manufacturing technology. *International Journal of Advanced Manufacturing Technology, 69,* 2269–2278.
4. Villafuerte, J. (2014). Considering cold spray for additive manufacturing. *Advanced Materials and Processes, 172,* 50–52.
5. Yin, S., Cavaliere, P., Aldwell, B., Jenkins, R., Liao, H., Li, W., & Lupoi, R. (2018). Cold spray additive manufacturing and repair: Fundamentals and applications. *Additive Manufacturing, 21,* 628–650.
6. Li, W., Yang, K., Yin, S., Yang, X., Xu, Y., & Lupoi, R. (2018). Solid-state additive manufacturing and repairing by cold spraying: A review. *Journal of Materials Science and Technology, 34,* 440–457.
7. Raoelison, R. N., Verdy, C., & Liao, H. (2017). Cold gas dynamic spray additive manufacturing today: Deposit possibilities, technological solutions and viable applications. *Materials and Design, 133,* 266–287.
8. Li, W., Cao, C., Wang, G., Wang, F., Xu, Y., & Yang, X. (2019, April). 'Cold spray +' as a new hybrid additive manufacturing technology: A literature review. *Science and Technology of Welding and Joining, 24*(5), 420–445. https://doi.org/10.1080/13621718.2019.1603851.
9. Huang, D., et al. (1991). Optical coherence tomography. *Science, 254*(5035), 1178–1181.
10. Dufour, M. L., Lamouche, G., Vergnole, S., Gauthier, B., Padioleau, C., Hewko, M., et al. (2006, September 8). Surface inspection of hard to reach industrial parts using low-coherence interferometry. In *Proceedings of SPIE, Photonics North 2006* (Vol. 6343, p. 63431Z).
11. Dufour, M. L., Lamouche, G., Detalle, V., Gauthier, B., & Sammut, P. (2005). Low-coherence interferometry—An advanced technique for optical metrology in industry. *Insight, 47,* 216.
12. Stifter, D. (2015). Nondestructive material testing using OCT. In W. Drexler & J. Fujimoto (Eds.), *Optical coherence tomography*. Cham: Springer.
13. Ji, Y., Grindal, A. W., Webster, P. J., & Fraser, J. M. (2015). Real-time depth monitoring and control of laser machining through scanning beam delivery system. *Journal of Physics D: Applied Physics, 48,* 155301.
14. Dupriez, N. D., & Truckenbrodt, C. (2016). OCT for efficient high quality laser welding. *Laser Technik Journal, 13,* 37–41.
15. Gardner, M. R., et al. (2018). In situ process monitoring in selective laser sintering using optical coherence tomography. *Optical Engineering, 57*(4), 041407.
16. Kanko, J. A., Sibley, A. P., & Fraser, J. M. (2016). In situ morphology-based defect detection of selective laser melting through inline coherent imaging. *Journal of Materials Processing Technology, 231,* 488–500.
17. Lévesque, D., Blouin, A., Néron, C., & Monchalin, J.-P. (2002). Performance of laser-ultrasonic F-SAFT imaging. *Ultrasonics, 40,* 1057–1063.
18. Kruger, S. E., Moreau, A., Lévesque, D., & Lord, M. (2001). Laser ultrasonic measurements of scattered waves in steel. In D. O. Thompson & D. E. Chimenti (Eds.), *Proceedings, Review of Progress in Quantitative Nondestructive Evaluation* (Vol. 20, pp. 1298–1305).
19. Karabutov, A. A., & Podymova, N. B. (2013). Nondestructive porosity assessment of CFRP composites with spectral analysis of backscattered laser-induced ultrasonic pulses. *Journal of Nondestructive Evaluation, 32,* 315–324.
20. Lobkis, O. I., Yang, L., Li, J., & Rokhlin, S. I. (2012). Ultrasonic backscattering in polycrystals with elongated single phase and duplex microstructures. *Ultrasonics, 52,* 694–705.

21. Legrand, N., et al. (2015). Laser-ultrasonic sensor to monitor steel microstructure at elevated temperature: Applications to hot rolling. In *Proceedings, 4th International Symposium on Laser Ultrasonics and Advanced Sensing (LU2015)*, Evanston, IL, paper #53.
22. Lévesque, D. (2017). Laser-ultrasonic methods to characterize steel microstructure: Overview and recent developments. In *3rd International Workshop on Laser-Ultrasound for Metals*, Stockholm, Sweden.
23. Vossen, J. L. (1978). Measurements of film-substrate bond strength by laser spallation. *American Society for Testing and Material Special Technical Publications, 640,* 122–133.
24. Gupta, V., et al. (1990). Measurement of interface strength by laser-pulse-induced spallation. *Materials Science and Engineering: A, 126,* 105–117.
25. Christoulis, D. K., et al. (2010). Cold-spraying coupled to nano-pulsed Nd-YaG laser surface pre-treatment. *Journal of Thermal Spray Technology, 19,* 1062–1073.
26. Arrigoni, M., et al. (2009). Laser Doppler interferometer based on a solid Fabry-Perot etalon for measurement of surface velocity in shock experiments. *Measurement Science & Technology, 20,* 015302.
27. Perton, M., Lévesque, D., Monchalin, J.-P., Lord, M., Smith, J. A., & Rabin, B. H. (2013). Laser shockwave technique for characterization of nuclear fuel plate interfaces. In D. O. Thompson & D. E. Chimenti (Eds.), *AIP Conference Proceedings. Proceedings, 39th Annual Review of Progress in Quantitative Nondestructive Evaluation*, Denver, CO (Vol. 1511, pp. 345–352).
28. Irissou, E., et al. (2008). Review on cold spray process and technology: Part I—Intellectual property. *Journal of Thermal Spray Technology, 17,* 495–516.
29. Christoulis, D. K., Jeandin, M., Irissou, E., Legoux, J.-G., & Knapp, W. (2012). Laser-assisted cold spray (LACS), Chapter 5. In: D. C. Dumitras (Ed.), *Nd:YAG laser* (pp. 59–96). Intech. ISBN: 978-953-51-0105-5.
30. Kruger, S. E., & Damm, E. B. (2006). Monitoring austenite decomposition by ultrasonic velocity. *Materials Science and Engineering: A, 425,* 238–243.
31. ASTM 681-08 Standard Specification for Tool Steels Alloy, ASTM International (Warrendale, PA), 2015.
32. Besler, R., Bauer, M., Furlan, K. P., Klein, A. N., & Janssen, R. (2017). Effect of processing route on the microstructure and mechanical properties of hot work tool steel. *Materials Research, 20*(6), 1518–1524. https://doi.org/10.1590/1980-5373-MR-2016-0726.